Chapter 8
Numerical Methods for Modelling and Simulation of Porous Materials

An Introduction Based on Finite Elements

Peter Goransson and Olivier Dazel

Abstract We introduce methods for modelling and simulation of anisotropic poroelastic materials in the frequency domain. Starting from the equations formulated by Biot, in their anisotropic form, we derive two different symmetric weak forms together with the boundary conditions that has to be satisfied. We employ a mixed displacement-pressure formulation and solutions are obtained by applying the finite element method to the proposed weak forms. In order to illustrate the use of the finite element method, we highlight some particular aspects related to simulations where poroelastic materials are involved. These include convergence of the discretised solution and boundary conditions at interfaces between poroelastic materials and solids/fluids. Results are given for some selected application examples of foam and plate combinations as well as a poroelastic foam with embedded inclusions.

8.1 Introduction

In flexible porous materials with open cells, the vibroacoustic energy is carried both through an airborne path, i.e. the sound pressure waves propagating through the fluid in the pores, and through an structure borne path, i.e. the elastic stress waves carried through the solid frame of the material. These waves are strongly coupled, i.e. they simultaneously propagate in both the fluid and the solid frame but with different strengths and relative phase. A characteristic of this coupled wave propagation, is that the vibroacoustic energy is dissipated and converted into heat as the wave travels through the material. To model such a dynamic behaviour, we use the elastic properties (i.e. stiffness controlled by material, topology, geometry, interfaces),

P. Goransson (✉)
KTH Royal Institute of Technology, Stockholm, Sweden
e-mail: pege@kth.se

O. Dazel
Laboratoire d'Acoustique de l'Université du Mans, UMR CNRS 6613, Le Mans Université, Avenue Olivier Messiaen, 72085 Le Mans, France
e-mail: olivier.dazel@univ-lemans.fr

N. Jiménez et al. (eds.), *Acoustic Waves in Periodic Structures, Metamaterials, and Porous Media*, Topics in Applied Physics 143,
https://doi.org/10.1007/978-3-030-84300-7_8

the viscoelastic properties (i.e. solid damping controlled by material, geometry), the acoustic properties (which are governed by the fluid medium) and the viscoacoustic properties (i.e. fluid damping controlled by geometry, topology, interfaces).

All these dissipation mechanisms are in general functions of frequency and furthermore, vary with frequency in strength and character. For a given situation, the balance between energy dissipated through vibration of the solid frame and changes in the acoustic pressure varies with the topological arrangement, choice of material properties, geometrical dimensions, interfacial conditions, etc. Traditionally, and also in the present work, the dynamic behaviour of porous materials is described in terms of macroscopic, space averaged quantities, such as acoustic pressure, elastic stress, solid and fluid displacements. In the current work parts of the modelling paradigm of porous foams, known in the literature as Biot's theory, will be briefly reviewed from an acoustics and vibrations perspective.

Traditional modelling and simulation of poroelastic materials (PEM) in vibroacoustic applications have for a long time been based on the assumption of isotropic elastic and acoustic properties, i.e. the materials possess a high degree of symmetry in their constitutive properties. However, it is well known that, due to the manufacturing processes involved, real PEMs are anisotropic to a certain degree. Examples where this holds are foamed polymers, fibrous wools etc. We will not review the large number of different methods that are available to solve problems involving isotropic PEM, for this we point to the recent review in [1]. Here we will instead start from Biot's equations in their anisotropic form, from which we derive and solve two different symmetric weak forms together with the boundary conditions that have to be satisfied in different configurations. Although there are a number of different choices of variables that can be made, the weak forms are here set up in terms of a mixed displacement-pressure formulation. The solutions are obtained by applying the finite element (FE) method.

To illustrate different aspects of modelling in applications where PEMs are involved, we solve some problems and results are given for selected application examples of a foam and plate combination. We highlight particular aspects related to convergence of the discretised solutions, boundary conditions at interfaces between poroelastic materials and solids/fluids, as well as solutions involving periodic boundary conditions and Bloch waves.

Our objective is to give a general introduction to the modelling of anisotropic PEM, however, without going into too much detail of the FE method as such, as this is beyond the scope of the present work. We will illustrate the effects of anisotropy with examples from the literature and we will show some intricate aspects of solving problems using simpler material models but still complex configurations. Our hope is that this will serve as a point of entry to the world of numerical modelling of these materials and an inspiration to go deeper into the subject.

8.2 Biot's Equations

The modelling considered here, is based on continuum mechanics at a mesoscopic scale, i.e. on homogenised fields of the porous materials. This is only possible if there exists a Representative Volume Element (RVE) whose size is sufficiently small in comparison with the wavelengths but also sufficiently large compared to the characteristic size of the heterogeneities to be representative. The motion of the solid (resp. fluid) part is averaged over the RVE and the homogenised media are called the solid and the fluid phase respectively.

The partial differential equations (PDEs) governing an anisotropic PEM involve (analogously to an isotropic material) coupling between the solid phase and the fluid phase in several different ways and the equation terms used to represent these interactions will be introduced below. The derivations take as a starting point the works by Biot [2–6]. Note that here but a brief introduction will be given, for more details see the literature cited throughout the text and the references provided therein. We define the necessary symbols as they are introduced in the derivation.

We start with some definitions and useful relations, in the form of the constitutive and the momentum equations. Recalling that the constitutive relations describe how the stresses relate to the deformation gradients, in both the solid and the fluid, there are coupling terms between the two phases related to the dilatation (compression) and deviation (shear). Similarly, the momentum equations which express the balance between internal forces, relate the gradients in the stress fields to the corresponding accelerations. These will be referred to as first order equations. We will identify frequency dependent quantities with a tilde symbol.

The expressions presented in this section originate from the theoretical framework proposed by Biot, [2, 5]. We will not recall the original equations stated by Biot as there are a large number of publications where they may be studied in close detail, see e.g. [7]. Instead most of the derivations that follow are inspired by [8], where the focus was on weak forms and FE, here presented in a slightly modified form.

In the original Biot theory, the modelling is based on the fluid homogenised displacements of the solid phase u_i^s and of the fluid phase u_i^f. The two corresponding stress tensors are σ^s and σ^f, which respectively represent the stress tensors of the solid and fluid phases, together forming the total stress $\sigma^t = \sigma^s + \sigma^f$. A few years after the original formulation, Biot proposed a modification to the original theory which was required to handle the case of inhomogeneous materials, in particular when the porosity is a function depending on space. The key was to replace the fluid displacement u_i^f by the relative flow $w_i = \phi(u_i^f - u_i^s)$, where ϕ is the open porosity.

From the basic relations proposed by Biot, a number of different representations may be proposed. For numerical modelling and solutions based on the FE method, where the computational effort required is strongly dependent on the number of *dof*, most of them keep the solid displacement and introduce the pressure as dependent field variables. This is directly related to one of the key properties of σ^f, i.e. that it is scalar and proportional to the acoustic pressure, through the relation $\sigma_{ij}^f = -\phi p \delta_{ij}$.

As will be shown below, using this, the fluid displacement and the fluid stress tensor may then be eliminated. This then leads to a new set of slightly modified solid displacements and stresses.

8.2.1 Constitutive Laws

In the following we will discuss the constitutive laws, here written in Cartesian tensor component notation, with Einstein's summation convention implied for repeated indices. Thus, with i, j the component ordinal numbers in Cartesian co-ordinate system, x_i with $i = 1, 2, 3$, $(.)_{,i} = \frac{\partial(.)}{\partial x_i}$ is the partial derivative with respect to co-ordinate x_i. δ_{ij} is the Kronecker's delta.

We begin with the constitutive laws for the solid,

$$\sigma_{ij}^s = \left(\hat{C}_{ijkl} + \frac{\tilde{Q}_{ij}\tilde{Q}_{kl}}{\phi^2 \tilde{K}_{eq}}\right)\varepsilon_{kl}^s + \tilde{Q}_{ij} u_{k,k}^f, \tag{8.1}$$

and for the fluid,

$$\sigma_{ij}^f = \left(\tilde{Q}_{kl}\varepsilon_{kl}^s + \phi^2 \tilde{K}_{eq} u_{k,k}^f\right)\delta_{ij}, \tag{8.2}$$

where ε_{kl}^s is the solid frame Cauchy strain tensor and $\hat{C}_{ijkl}$ corresponds to the *in-vacuo* Hooke tensor of the solid phase. As shown in [8], K_{eq} is the scalar fluid compressibility modulus:

$$\tilde{K}_{eq} = \frac{K_s}{1 - \phi - K_s \tilde{C}_{ijkl} d_{ij} d_{kl} + \phi K_s / K_f}, \quad d_{ij} = -\frac{\varepsilon_{ij}^s}{p} \tag{8.3}$$

where d_{ij} is the unjacketed frame compressibility compliance tensor. Furthermore, $\tilde{Q}_{ij}$ is the dilatational coupling tensor:

$$\tilde{Q}_{ij} = \frac{\left[(1-\phi)\,\delta_{ij} - \tilde{C}_{ijkl} d_{kl}\right]\phi K_s}{1 - \phi - K_s \tilde{C}_{ijkl} d_{ij} d_{kl} + \phi K_s / K_f}. \tag{8.4}$$

Two other stress tensors may also be considered. The total stress tensor σ^t and the *in-vacuo* stress tensor of the solid phase, which corresponds to the stress in the absence of fluid: $\hat{\sigma}_{ij}^s = \hat{C}_{ijkl}\varepsilon_{kl}^s$. These are linked by the following relations:

$$\sigma_{ij}^t = \sigma_{ij}^s + \sigma_{ij}^f = \hat{\sigma}_{ij} - \tilde{\gamma}'_{ij} p, \quad , \tag{8.5}$$

where $\tilde{\gamma}'_{ij}$ is an elastic coupling coefficient,

$$\tilde{\gamma}'_{ij} = \phi\left(\delta_{ij} + \frac{\tilde{Q}_{ij}}{\phi^2 \tilde{K}_{eq}}\right), \tag{8.6}$$

which may be used to express the link between the solid and *in-vacuo* stress tensors:

$$\sigma^s_{ij} = \hat{\sigma}^s_{ij} - \left(\tilde{\gamma}'_{ij} - \phi\delta_{ij}\right) p. \tag{8.7}$$

The pressure p is related to the divergence of the fluid displacement u^W,

$$p = -\tilde{K}_{eq} u^W_{j,j}, \tag{8.8}$$

where u^W is a combination of the solid and fluid displacement defined as,

$$u^W_j = \phi\left(u^f_j + \frac{\tilde{Q}_{jl}}{\phi^2 \tilde{K}_{eq}} u^s_l,\right) \tag{8.9}$$

which is equivalent to,

$$u^f_j = \frac{u^W_j}{\phi} - \frac{\tilde{Q}_{jl}}{\phi^2 \tilde{K}_{eq}} u^s_l. \tag{8.10}$$

Thus, using (8.10), we may replace the fluid displacement by a combination of u^W and the gradient of the pressure.

8.2.2 Momentum Equations

The momentum equations were given in [8] as:

$$\sigma^s_{ij,j} = -\omega^2 \tilde{\rho}^{11}_{ij} u^s_j - \omega^2 \tilde{\rho}^{12}_{ij} u^f_j, \tag{8.11}$$

and

$$\sigma^f_{ij,j} = -\omega^2 \tilde{\rho}^{12}_{ij} u^s_j - \omega^2 \tilde{\rho}^{22}_{ij} u^f_j. \tag{8.12}$$

As in the original Biot's formulation, these equations involve three complex densities. In order to simplify the expressions, especially as now we have tensors (as opposed to scalars for an isotropic material) that will be inverted and multiplied, we choose to express all of them through the dynamic tortuosity, $\tilde{\alpha}_{ij}$,

$$\tilde{\rho}^{22}_{ij} = \phi\rho_0\tilde{\alpha}_{ij}, \quad \tilde{\rho}^{12}_{ij} = \phi\rho_0\left(\delta_{ij} - \tilde{\alpha}_{ij}\right), \quad \tilde{\rho}^{11}_{ij} = \rho_1 + \phi\rho_0\left(\tilde{\alpha}^{\infty}_{ij} - \delta_{ij}\right), \tag{8.13}$$

with

$$\tilde{\alpha}_{ij} = \alpha^{\infty}_{ij} - j\frac{\tilde{b}_{ij}}{\omega}, \tag{8.14}$$

and α_{ij}^{∞} being the geometric tortuosity tensor and $\tilde{b}_{ij}$ the viscous drag tensor. One may now take advantage of the scalar property of the fluid stress tensor, to express the fluid displacement u^f as a function of the solid displacement and the pressure. This leads to a second relation which allows us to replace the fluid displacement:

$$u_j^f = \frac{\hat{\alpha}_{jk} p_{,k}}{\phi \rho_0 \omega^2} + (\delta_{jk} - \hat{\alpha}_{jk}) u_k^s, \tag{8.15}$$

where $\hat{\alpha}_{jk}$ is the inverse of the dynamic tortuosity tensor ($\hat{\alpha}_{ik}\tilde{\alpha}_{kj} = \delta_{ij}$).

From this, we may rewrite the solid momentum equation as:

$$\hat{\sigma}_{ij,j}^s + \tilde{\gamma}_{ij} p_{,j} = -\omega^2 \tilde{\rho}_{ij} u_j^s, \tag{8.16}$$

with

$$\tilde{\gamma}_{ij} = \phi \hat{\alpha}_{ij} - \tilde{\gamma}'_{ij}, \tag{8.17}$$

$$\tilde{\rho}_{ij} = \rho_1 + \phi \rho_0 (\delta_{ij} - \hat{\alpha}_{ij}), \tag{8.18}$$

where $\tilde{\gamma}_{ij}$ is a coupling factor which involves dynamic effects through the dynamic tortuosity and elastic coupling through $\tilde{\gamma}'_{ij}$. Note that $\tilde{\rho}_{ij}$ is the solid apparent density.

In a similar way the fluid displacement may be eliminated from the fluid momentum equation using the displacement u_i^W:

$$-\phi^2 p_{,i} = -\omega^2 \phi \rho_0 \left(\delta_{ij} - \tilde{\alpha}_{ij} + \frac{\tilde{\alpha}_{ik} \tilde{Q}_{kj}}{\phi^2 \tilde{K}_{eq}} \right) u_j^s - \omega^2 \rho_0 \tilde{\alpha}_{ij} u_j^W, \tag{8.19}$$

We may condense this relation through rewriting it as,

$$-\frac{\phi^2}{\rho_0 \omega^2} \hat{\alpha}_{ij} p_{,j} = -\tilde{\gamma}_{ij} u_j^s - u_i^W, \tag{8.20}$$

The advantage of considering u_i^W is that it may now be eliminated by taking the divergence and introducing (8.8),

$$-\frac{\phi^2}{\rho_0 \omega^2} \hat{\alpha}_{ij} p_{,ji} = -\tilde{\gamma}_{ij} u_{j,i}^s + \frac{p}{\tilde{K}_{eq}}. \tag{8.21}$$

We have with these relations completed the transformation from fluid stress tensor and displacements, to pressure and solid displacements for the anisotropic PEM modelling.

8.3 Weak Forms

There are a number of different ways of setting up the weak forms for an anisotropic PEM. Although in principle equal, slightly different choices may be made in the derivations. These choices introduce boundary terms that may lead to natural, homogeneous coupling conditions that may be of interest in certain applications. Frequently we face modelling situations where a PEM is placed next to a solid panel, or when it is in direct contact to an air domain, but there are of course other configurations that could be considered as well. Here, two mixed displacement formulations will be presented, one which naturally couples with an acoustic air domain, see [9] for the isotropic PEM modelling, (here referred to as the air formulation or PEM1) and one which naturally couples with a solid in the case where the solid displacements are continuous and the normal relative flow is zero, see [10] for the isotropic PEM modelling, (here referred to as the bonded solid formulation or PEM2).

8.3.1 PEM1 Weak Formulation

To state the weak forms, we introduce the test functions v_i^s and q. We start with the solid momentum equations, (8.16), and multiply by v_i^s, integrate over the porous domain Ω of boundary Γ_p and perform a partial integration of the solid stress gradient term. This gives,

$$\int_{\Omega} v_{i,j}^s \hat{C}_{ijkl} u_{k,l}^s - \omega^2 v_i^s \tilde{\rho}_{ij} u_j^s + v_i^s \tilde{\gamma}_{ij} p_{,j} \, \mathrm{d}\Omega = \int_{\Gamma} v_i^s \hat{\sigma}_{ij}^s n_j \, \mathrm{d}\Gamma. \tag{8.22}$$

Similarly we multiply equation (8.21) by q, integrate over the porous domain Ω_p and perform a partial integration of the term involving the second order gradient of the pressure,

$$\int_{\Omega} \frac{\phi^2}{\rho_0 \omega^2} \hat{\alpha}_{ij} p_{,j} q_{,i} - \frac{pq}{\tilde{K}_{eq}} + \tilde{\gamma}_{ij} u_{j,i}^s q \, \mathrm{d}\Omega = \int_{\Gamma} \frac{\phi^2}{\rho_0 \omega^2} \hat{\alpha}_{ij} p_{,j} n_i q \, \mathrm{d}\Gamma. \tag{8.23}$$

As will be shown later, these two equations naturally couples with a weak form representing air through the boundary integral on their respective RHS. It will in the following be referred to as PEM1.

8.3.2 PEM2 Weak Formulation

The objective of the second formulation is to modify the weak form in order to introduce slightly different boundary integral terms that naturally couples with a

solid attached panel. We start by rewriting the third term on the LHS of (8.22), using (8.18) and performing a partial integration, as

$$\int_\Omega v_i^s \tilde{\gamma}_{ij} p_{,j}\, d\Omega = \int_\Omega \phi v_i^s \hat{\alpha}_{ij} p_{,j}\, \mathrm{d}\Omega + \tilde{\gamma}'_{ij} \left(\int_\Omega v_{i,j}^s p\, d\Omega - \int_\Gamma v_i^s \delta_{ij} n_j p\, \mathrm{d}\Gamma \right).$$

This allows us to rewrite the weak form of the solid part as,

$$\int_\Omega v_{i,j}^s \hat{C}_{ijkl} u_{k,l}^s - \omega^2 v_i^s \tilde{\rho}_{ij} u_j^s + \phi v_i^s \hat{\alpha}_{ij} p_{,j} + \tilde{\gamma}'_{ij} v_{i,j}^s p\, d\Omega = \int_\Gamma v_i^s \hat{\sigma}_{ij}^t n_j\ \mathrm{d}\Gamma, \quad (8.24)$$

Similarly, for the third term of the LHS of (8.23), we may write,

$$\int_\Omega \tilde{\gamma}_{ij} u_{j,i}^s q\, d\Omega = \int_\Omega \phi \hat{\alpha}_{ij} u_{j,i}^s q\, d\Omega + \left(\int_\Omega \tilde{\gamma}'_{ij} u_i^s q_{,j}\, d\Omega - \int_\Gamma p \delta_{ij} v_i^s n_j\, \mathrm{d}\Gamma \right) d\Gamma,$$

and the weak form of the fluid is then,

$$\int_\Omega \frac{\phi^2}{\rho_0 \omega^2} \hat{\alpha}_{ij} p_{,i} q_{,j} - \frac{pq}{\tilde{K}_{eq}} + \tilde{\gamma}'_{ij} u_{j,i}^s q + \phi \hat{\alpha}_{ij} u_{j,i}^s q\, d\Omega = \int_\Gamma q w_j n_j q\ \mathrm{d}\Gamma. \quad (8.25)$$

In these forms, the above two equations naturally couples with a weak form representing a solid through the boundary integral on their respective RHS. This formulation will in the following be referred to as PEM2.

8.3.3 Elastic Solid

In order to prepare for the discussion of the coupling between different types of domains in more detail, we introduce the weak form for the elastic structure as

$$\int_{\Omega_p} v_{i,j}^e C_{ijkl}^e u_{k,l}^e - \rho_e \omega^2 v_i^e u_j^e\, \mathrm{d}\Omega = \int_\Gamma v_i^s \hat{\sigma}_{ij}^e n_j^e\, \mathrm{d}\Gamma, \quad (8.26)$$

where u^e and v^e are respectively the unknown elastic solid displacements and the corresponding test fields. Furthermore, $\hat{\sigma}_{ij}^e = C_{ijkl}^e u_{k,l}^e$ is the stress tensor of the elastic structure, ρ_e is its density and n^e is the outgoing normal of the elastic domain.

8.3.4 Air

Finally, to conclude this part discussing weak forms, the air cavity weak form is,

$$\int_{\Omega_i} \frac{p^a_{,j} q^a_{,j}}{\rho_a \omega^2} - \frac{p^a q^a}{K_a} \, \mathrm{d}\Omega = \int_{\Gamma_i} \frac{1}{\rho_a \omega^2} q^a p^a_{,j} n^a_j \, \mathrm{d}\Gamma, \tag{8.27}$$

where p_a is the acoustic pressure in the air domain, K_a is the bulk modulus of air, ρ_a the ambient density of air, n^a is the outgoing normal of the acoustic domain and q_a the test field.

8.4 Discrete Linear System

To obtain a FE based solution of a problem involving, among others PEMs, we start from the weak forms presented in (8.3). The steps required to obtain the discretisation are the same as for elastic structures and acoustic domains etc., and we will only recall the PEM case here.

First we divide the domain into a finite number of, non-overlapping domains, commonly referred to as elements, denoted by Ω_e with $e = 1...N_e$. These elements form a mesh and in each of them the PDEs are transformed into algebraic equations, which are approximations to the exact solution. The elements are preferably simple in shape, thus requiring a finite set of polynomial shape functions to sufficiently accurate describe the variation of the field variables in the sub-domain. Typical functions used are nodal or bubble shape functions along edges, faces and in the interior. Some examples (Lobatto shape functions) are given in the following.

With simple polynomial shape functions, the element equations may be numerically integrated, resulting in elementary matrices that approximate the spatial variation, and then assembled into a larger system of algebraic equations, which then may be solved numerically and the solution obtained may be used to obtain relevant results such as pressures, displacements, etc.

8.4.1 Elementary Matrices

Assuming that we have N_d shape functions in an element e, a physical field $f^{(e)}$ may be approximated by:

$$f^{(e)}(\mathbf{x}) \approx \sum_{k=1}^{N_d} \varphi_k(\mathbf{x}) f_k^{(e)} = [\boldsymbol{\varphi}(\mathbf{x})]\mathbf{f}^{(e)}. \tag{8.28}$$

The shape functions $\varphi_k(\mathbf{x})$ approximate the spatial dependence of the fields, and usually the test fields, v_i^s and q, are approximated in a similar manner. Each shape function is associated to a degree of freedom f_k^e which will be an unknown of the global FE problem. The shape functions and degrees of freedom of one element can be respectively gathered in a matrix $[\boldsymbol{\varphi}(\mathbf{x})]$ and a vector $\mathbf{f}^e$.

The key characteristic of a poroelastic material is that four fields should be discretised (three displacement fields and one pressure fields). We then have, for the pressure:

$$p^{(e)}(\mathbf{x}) \approx [\boldsymbol{\varphi}(\mathbf{x})]\mathbf{p}^{(e)}, \tag{8.29}$$

and for the displacements, where each direction is discretised independently,

$$\begin{Bmatrix} u_1^{(e)}(\mathbf{x}) \\ u_2^{(e)}(\mathbf{x}) \\ u_3^{(e)}(\mathbf{x}) \end{Bmatrix} = \underbrace{\begin{bmatrix} [\boldsymbol{\varphi}(\mathbf{x})] & 0 & 0 \\ 0 & [\boldsymbol{\varphi}(\mathbf{x})] & 0 \\ 0 & 0 & [\boldsymbol{\varphi}(\mathbf{x})] \end{bmatrix}}_{[\boldsymbol{\varphi}_{\mathbf{u}}(\mathbf{x})]} \mathbf{u}^{(e)}, \quad \mathbf{u}^{(e)} = \begin{Bmatrix} \mathbf{u}_1^{(e)} \\ \mathbf{u}_2^{(e)} \\ \mathbf{u}_3^{(e)} \end{Bmatrix}. \tag{8.30}$$

The dynamics of the response of the PEM in one element is then approximated in terms of elementary vectors $\mathbf{u}^{(e)}$ and $\mathbf{p}^{(e)}$. Note that here we have chosen to use the same shape functions for the pressure and the three displacements fields. However, this is not a requirement as different shape functions (or different orders) can be considered for each unknown.

8.4.2 Discretisation of the Weak Forms in One Element

The discretisation of the 8 volume integral terms (4 for the solid and four for the pressure), that appear for both the PEM1 and the PEM2 formulations, is assumed to be the same. Most of the integrals involved are standard for any FE problem and will not be detailed here. Instead, we will present the discretisation for the terms which are typical for PEM modelling, i.e. the corresponding volumetric coupling between the solid and fluid phases. Note that in this section, we mix the summation convention and matrix forms and it should be clear from the context when one or the other is used. We start with the discretisation of the third term of the LHS of (8.24):

$$\int_{\Omega_{(e)}} v_i^s \hat{\alpha}_{ij} p_{,j} \, \mathrm{d}\Omega \approx \int_{\Omega_{(e)}} \mathbf{v}_i^{(e)^T} [\boldsymbol{\varphi}_{\mathbf{u}}(\mathbf{x})]^T \hat{\alpha}_{ij} [\boldsymbol{\varphi}_{,j}(\mathbf{x})] \mathbf{p}^{(e)} \, \mathrm{d}\Omega. \tag{8.31}$$

Note that the term corresponding to the test field has been transposed, this allows us to separate the vectors $\mathbf{v}^{(e)}$ and $\mathbf{p}^{(e)}$ from the integral. This leads to the definition of a volume coupling matrix $[\mathbf{C}_{(e)}]$ which is a $(3N_d \times N_d)$ matrix as:

$$[\mathbf{C}^1_{(e)}] = \int_{\Omega_{(e)}} [\boldsymbol{\varphi}_{\mathbf{u}}(\mathbf{x})]^T \hat{\alpha}_{ij} [\boldsymbol{\varphi}_{,j}(\mathbf{x})] \, \mathrm{d}\Omega. \tag{8.32}$$

The superscript 1 is introduced to distinguish this particular form of the coupling matrix from other coupling terms, that will be discussed below. The discretisation of the coupling term over an element will then lead to:

$$\int_{\Omega_{(e)}} v^s_i \hat{\alpha}_{ij} p_{,j} \, \mathrm{d}\Omega \approx \mathbf{v}^{(e)^T} [\mathbf{C}^1_{(e)}] \mathbf{p}^{(e)}. \tag{8.33}$$

Similarly for the fourth term of the LHS of (8.24), another $(3N_d \times N_d)$ matrix $[\mathbf{C}^2_{(e)}]$ is introduced as:

$$\int_{\Omega_{(e)}} \tilde{\gamma}'_{ij} v^s_{i,j} p \, \mathrm{d}\Omega \approx \mathbf{v}^{(e)^T} [\mathbf{C}^2_{(e)}] \mathbf{p}^{(e)}, \tag{8.34}$$

Finally there is yet one more coupling term, i.e. the third one in the LHS of (8.22), which is discretised as:

$$\int_{\Omega_{(e)}} v^s_i \hat{\gamma}_{ij} p_{,j} \, \mathrm{d}\Omega \approx \mathbf{v}^{(e)^T} [\mathbf{C}^3_{(e)}] \mathbf{p}^{(e)}. \tag{8.35}$$

Without going into further details of the derivations, we apply the same methodology to the other terms which are common between the two different formulations:

$$\int_{\Omega_{(e)}} v^s_{i,j} \hat{C}_{ijkl} u^s_{k,l} \, \mathrm{d}\Omega \approx \mathbf{v}^{(e)^T} [\mathbf{K}_{(e)}] \mathbf{u}^{(e)}, \quad \int_{\Omega_{(e)}} v^s_i \tilde{\rho}_{ij} u^s_j \, \mathrm{d}\Omega \approx \mathbf{v}^{(e)^T} [\mathbf{M}_{(e)}] \mathbf{u}^{(e)},$$

$[\mathbf{K}_{(e)}]$ and $[\mathbf{M}_{(e)}]$ are the elementary stiffness and mass matrices. For terms relative to the fluid, one has:

$$\int_{\Omega_{(e)}} \frac{\phi^2}{\rho_0} \hat{\alpha}_{ij} p_{,j} q_{,j} \, \mathrm{d}\Omega \approx \mathbf{q}^{(e)^T} [\mathbf{H}_{(e)}] \mathbf{p}^{(e)}, \quad \int_{\Omega_{(e)}} \frac{pq}{\tilde{K}_{eq}} \, \mathrm{d}\Omega \approx \mathbf{q}^{(e)^T} [\mathbf{q}_{(e)}] \mathbf{p}^{(e)},$$

$[\mathbf{H}_{(e)}]$ and $[\mathbf{Q}_{(e)}]$ are the elementary kinetic and compression energy matrices which are also common to the two weak forms. Note that all integrals above are in practice computed for a standard reference element, and scaled to the actual element geometry.

The full elementary dynamic matrix $[\mathbf{A}_{(e)}]$ for the PEM1 formulation, is then

$$[\mathbf{A}_{(e)}] = \left[\begin{array}{c|c} [\mathbf{K}_{(e)}] - \omega^2 [\mathbf{M}_e] & [\mathbf{C}^3_{(e)}] \\ \hline [\mathbf{C}^3_{(e)}]^T & \dfrac{[\mathbf{H}_{(e)}]}{\omega^2} - [\mathbf{Q}_{(e)}] \end{array}\right]. \tag{8.36}$$

For the PEM2 formulation where $\{\mathbf{u}, \mathbf{p}\}$ naturally couples to a solid, we have

$$[\mathbf{A}'_{(e)}] = \left[\begin{array}{c|c} [\mathbf{K}_{(e)}] - \omega^2[\mathbf{M}_e] & [\mathbf{C}^1_{(e)}] + [\mathbf{C}^2_{(e)}] \\ \hline [\mathbf{C}^1_{(e)}]^T + [\mathbf{C}^2_{(e)}]^T & \dfrac{[\mathbf{H}_{(e)}]}{\omega^2} - [\mathbf{Q}_{(e)}] \end{array}\right]. \tag{8.37}$$

We see that the two formulations differ by the coupling terms between the solid and the fluid, but otherwise have the same structure. Thus, in the following parts of the procedure, as most of the steps are common between the two formulations, we have decided not to overload the notation and instead to use a generic form as,

$$[\mathbf{A}_{(e)}] = \begin{bmatrix} [\mathbf{A}^{uu}_{(e)}] & [\mathbf{A}^{up}_{(e)}] \\ [\mathbf{A}^{pu}_{(e)}] & [\mathbf{A}^{pp}_{(e)}] \end{bmatrix}. \tag{8.38}$$

8.4.3 Assembly

The global system matrices, required to complete the modelling for a complex problem consisting of many elements, are obtained by summation of elementary matrices and the method is the same for the two formulations. This is in principle not different from any other FE solution, but some extra attention needs to be paid to the matching between different degrees of freedom to their proper neighbours. As the vector of degrees of freedom for a particular element $\{\mathbf{u}^{(e)}, \mathbf{p}^{(e)}\}$ is a sub-vector of the global vector of degrees of freedom $\{\mathbf{u}, \mathbf{p}\}$, we need to establish a correspondence. There are several ways of doing this, one is to introduce a boolean matrix $[\mathbf{L}^{(e)}]$ of dimension $(4N_d \times 4N_g)$ where $4N_g$ corresponds to the total number of degrees of freedom. We then have:

$$\begin{Bmatrix} \mathbf{u}^{(e)} \\ \mathbf{p}^{(e)} \end{Bmatrix} = [\mathbf{L}_e] \begin{Bmatrix} \mathbf{u} \\ \mathbf{p} \end{Bmatrix}. \tag{8.39}$$

The global dynamic matrix then reads:

$$[\mathbf{A}] = \sum_{e=1}^{N} [\mathbf{L}^{(e)}]^T [\mathbf{A}_{(e)}][\mathbf{L}^{(e)}] = \begin{bmatrix} [\mathbf{A}^{uu}] & [\mathbf{A}^{up}] \\ [\mathbf{A}^{pu}] & [\mathbf{A}^{pp}] \end{bmatrix}. \tag{8.40}$$

Note that this way of approaching the assembly is purely formal and just used to explain the principles involved. Indeed, it can be shown that the multiplication $[\mathbf{L}^{(e)}]^T[\mathbf{A}_{(e)}][\mathbf{L}^{(e)}]$ is a matrix of size $(4N_g \times 4N_g)$ with a submatrix corresponding to $[\mathbf{A}_{(e)}]$ at the position corresponding to the *dof* of the element. The global matrix is then composed of four blocks which are the assembly of the elementary ones.

8.5 Coupling Between Domains

We will in the following discuss how a FE-PEM domain is assembled into a more complex arrangement of different media, such as a solid and a fluid. As part of this we will also illustrate the difference between the two weak formulations derived.

8.5.1 Coupling with an Air Domain

First we consider the problem of coupling between an acoustic domain and a poroelastic one, see Fig. 8.1 where the two domains are artificially separated to clearly illustrate the coupling between the two. The degrees of the acoustic domain correspond to the pressure. At the boundary Γ between the two domains, a compatible mesh is considered and the common pressure degrees of freedom are denoted $\mathbf{p}_\Gamma$, hence the *dof* of the two media can be partitioned as $\{\mathbf{u}, \mathbf{p}_i, \mathbf{p}_\Gamma\}$ for the PEM where $\mathbf{p}_i$ correspond to the vector of pressure in the interior of the domain. For the fluid domain, the *dof* are similarly $\{\mathbf{p}_\Gamma, \mathbf{p}_i^a\}$.

We now partition the generic global dynamic PEM matrix (8.40) into three blocks in order to introduce the partitioning between the boundary and interior *dof*. Applying the same partitioning to the test fields, the weak form is then approximated by:

$$\begin{bmatrix}\mathbf{v}^T & \mathbf{q}_i{}^T & \mathbf{q}_\Gamma{}^T\end{bmatrix}\begin{bmatrix}[\mathbf{A}^{uu}] & [\mathbf{A}_i^{up}] & [\mathbf{A}_\Gamma^{up}]\\ [\mathbf{A}_i^{pu}] & [\mathbf{A}_{ii}^{pp}] & [\mathbf{A}_{i\Gamma}^{pp}]\\ [\mathbf{A}_\Gamma^{pu}] & [\mathbf{A}_{\Gamma i}^{pp}] & [\mathbf{A}_{\Gamma\Gamma}^{pp}]\end{bmatrix}\begin{Bmatrix}\mathbf{u}\\ \mathbf{p}_i\\ \mathbf{p}_\Gamma\end{Bmatrix}. \tag{8.41}$$

The weak form for the air cavity is given in (8.27). Note that the outgoing normal n^a is in the opposite direction of n^p. The volume integrals, for the air domain may then be discretised as discussed above and a dynamic acoustic matrix, which may also be partitioned between boundary and interior *dof* , is then:

$$\begin{bmatrix}\mathbf{q}_\Gamma{}^T & \mathbf{q}_i^{aT}\end{bmatrix}\begin{bmatrix}[\mathbf{A}_{\Gamma\Gamma}^a] & [\mathbf{A}_{\Gamma i}^a]\\ [\mathbf{A}_{i\Gamma}^a] & [\mathbf{A}_{ii}^a]\end{bmatrix}\begin{Bmatrix}\mathbf{p}_\Gamma\\ \mathbf{p}_i^a\end{Bmatrix}. \tag{8.42}$$

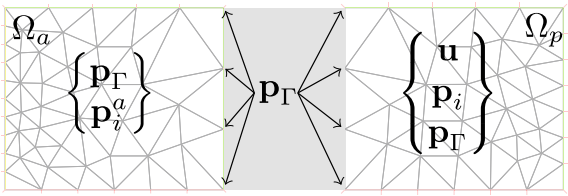

Fig. 8.1 Coupling of acoustic and poroelastic FE models

Adding the two discretised weak forms, air and PEM, leads to:

$$\begin{bmatrix}\mathbf{v}^T & \mathbf{q}_i{}^T & \mathbf{q}_\Gamma{}^T & \mathbf{q}_i^{a\,T}\end{bmatrix}\begin{bmatrix}[\mathbf{A}^{uu}] & [\mathbf{A}_i^{up}] & [\mathbf{A}_\Gamma^{up}] & [\mathbf{0}]\\ [\mathbf{A}_i^{pu}] & [\mathbf{A}_{ii}^{pp}] & [\mathbf{A}_{i\Gamma}^{pp}] & [\mathbf{0}]\\ [\mathbf{A}_\Gamma^{pu}] & [\mathbf{A}_{\Gamma i}^{pp}] & [\mathbf{A}_{\Gamma\Gamma}^{pp}]+[\mathbf{A}_{\Gamma\Gamma}^{a}] & [\mathbf{A}_{\Gamma i}^{a}]\\ [\mathbf{0}] & [\mathbf{0}] & [\mathbf{A}_{i\Gamma}^{a}] & [\mathbf{A}_{ii}^{a}]\end{bmatrix}\begin{Bmatrix}\mathbf{u}\\ \mathbf{p}_i\\ \mathbf{p}_\Gamma\\ \mathbf{p}_i^a\end{Bmatrix}. \tag{8.43}$$

We can deduce from this expression that, as for the assembly of elements, the global matrix which is the assembly of the two domains may be done by summing the overlapping parts of the dynamic matrices.

So far we have treated the volumetric terms in the weak forms and, as pointed out before, there is no difference between the two up to now. What remains is to derive the interface terms, and how they should be discretised. Here we have to distinguish between the two formulations, PEM1 and PEM2, as we will show below. However, let us first consider the interface relations between the different physical fields at the common boundary. Along Γ the pressure has to be continuous, the normal displacement of air has to be equal to the normal total displacement of the porous medium and, finally, as the solid frame of the PEM is free, the *in-vacuo* solid frame stress of the PEM has to vanish:

$$p^a = p, \quad \hat{\sigma}_{ij}^s n_j = 0, \quad \frac{p^a_{,j} n_j}{\rho_a \omega^2} = u_n^a = u_n^t = \frac{\phi^2 \hat{\alpha}_{ij} p_{,j} n_i}{\rho_0 \omega^2}. \tag{8.44}$$

If we now consider the case of the PEM1 formulation, that naturally should couple with air, the sum of the boundary terms associated to the PEM are,

$$\int_{\Gamma_i} v_i^s \hat{\sigma}_{ij}^s n_j + \frac{\phi^2}{\rho_0 \omega^2} \hat{\alpha}_{ij} p_{,j} n_i \, \mathrm{d}\Gamma. \tag{8.45}$$

The first term is zero as the *in-vacuo* stress is null at the interface. Concerning the second one, let us combine the terms relative to the cavity and the PEM in one integral expression. We then have:

$$\int_\Gamma \left(\frac{\phi^2}{\rho_0 \omega^2} \hat{\alpha}_{ij} p_{,j} n_i q - \frac{1}{\rho_a \omega^2} q^a p^a_{,j} n_j \right) \mathrm{d}\Gamma, \tag{8.46}$$

where the minus sign for the air term is due to the orientation of the normals. As we are only dealing with the case of compatible meshes, q^a and q are identical and we can deduce the nullity of this integral by the continuity of normal displacements, (8.44). Hence, for this $\{\mathbf{u}, \mathbf{p}\}$ formulation, the coupling with an acoustic domain is natural (which means that there is no surface term). The degrees of freedom of the global problem correspond to the merging of the acoustic pressures in the air domain $\mathbf{p}^a$ and the displacement $\mathbf{u}$ and pressure $\mathbf{p}$ of the PEM. We see that the porous material and the acoustic air have common degrees of freedom.

For the PEM2 formulation, the boundary terms are

$$\int_{\Gamma} \left(v_i^s \hat{\sigma}_{ij}^t n_j + q w_j n_j - \frac{1}{\rho_a \omega^2} q^a p_{,j}^a n_j \right) \mathrm{d}\Gamma. \tag{8.47}$$

However, as the *in-vacuo* stress tensor is zero, one has that $\hat{\sigma}_{ij}^t = -p\delta_{ij}$ and due to the continuity of pressure along Γ, we can replace the total stress by the pressure of air. In addition

$$q w_j n_j - \frac{1}{\rho_a \omega^2} q^a p_{,j}^a n_j = q^a \left(u_j^t - u_j^s - u_j^a \right) n_j = -q^a u_j^s n_j. \tag{8.48}$$

The combined boundary terms are then:

$$-\int_{\Gamma} p^a v_j^s n_j + q^a u_j^s n_j \, \mathrm{d}\Gamma. \tag{8.49}$$

This term is a standard fluid structure interaction couple and its discretisation leads to a coupling matrix $[\boldsymbol{\Gamma}_{fs}]$ between the solid displacement of the porous material and the pressure in air which should be added to the global matrix. The system matrix will then be:

$$\begin{bmatrix} [\mathbf{A}^{uu}] & [\mathbf{A}_i^{up}] & [\mathbf{A}_\Gamma^{up}] - [\boldsymbol{\Gamma}_{fs}] & [\mathbf{0}] \\ [\mathbf{A}_i^{pu}] & [\mathbf{A}_{ii}^{pp}] & [\mathbf{A}_{i\Gamma}^{pp}] & [\mathbf{0}] \\ [\mathbf{A}_\Gamma^{pu}] - [\boldsymbol{\Gamma}_{fs}]^T & [\mathbf{A}_{\Gamma i}^{pp}] & [\mathbf{A}_{\Gamma\Gamma}^{pp}] + [\mathbf{A}_{\Gamma\Gamma}^{a}] & [\mathbf{A}_{\Gamma i}^{a}] \\ [\mathbf{0}] & [\mathbf{0}] & [\mathbf{A}_{i\Gamma}^{a}] & [\mathbf{A}_{ii}^{a}] \end{bmatrix}. \tag{8.50}$$

The coupling between an air domain and this form of the $\{\mathbf{u}, \mathbf{p}\}$ formulation is thus not natural as we need the additional term $[\boldsymbol{\Gamma}_{fs}]$.

8.5.2 Coupling with an Elastic Solid

The coupling of a PEM domain and an elastic structural domain can be done in a similar way. The weak form for the elastic solid structure is given by (8.26). Note that, n^e in each point along the interface is in a direction opposite to the one of the poroelastic material. The interface relations at such an interface are:

$$\sigma_{ij}^e = \hat{\sigma}_{ij} - p\delta_{ij}, \quad u_j^e = u_j^s. \tag{8.51}$$

Let us first consider the PEM2 formulation, which we have previously claimed to naturally couple with a solid. The boundary terms are

$$\int_{\Gamma} \left(v_i^s \sigma_{ij}^t n_j + q w_j n_j - v_i^e \hat{\sigma}_{ij}^e n_j \right) \mathrm{d}\Gamma. \tag{8.52}$$

Similarly to the previous case compatible meshes are considered, and we then have $v_i^e = v_i^s$. In addition $w_j n_j = (u_j^t - u_j^s) n_j = 0$. Hence the boundary integral is zero meaning that the coupling between an elastic structure and this PEM2 formulation is natural. Similarly to the coupling between PEM1 and an air domain, the dynamic equation system is obtained by summing the matrix terms corresponding to common *dof* along Γ.

For the PEM1 formulation in Sect. 8.3.1, the surface term is given as:

$$\int_\Gamma \left(v_i^s \left(\hat{\sigma}_{ij} - \hat{\sigma}_{ij}^e \right) n_j + q \frac{\phi^2}{\rho_a \omega^2} \hat{\alpha}_{ij} p_{,j} n_i \right) \mathrm{d}\Gamma. \tag{8.53}$$

The interface conditions of interest are

$$\hat{\sigma}_{ij} - \sigma_{ij}^e = p \delta_{ij}, \quad u_i^e n_i = \frac{\phi^2}{\rho_a \omega^2} \hat{\alpha}_{ij} p_{,j} n_i. \tag{8.54}$$

The boundary integral is then finally:

$$- \int_\Gamma \left(p v_j^s n_j + q u_j^s n_j \right) \mathrm{d}\Gamma, \tag{8.55}$$

which is similar to (8.49), and the assembled equation system is obtained by adding the *dof* corresponding to the Γ and adding the coupling terms in a way similar to what is shown in (8.50).

8.5.3 Coupling Through a Thin Airgap Interface

Quite often, the interface between a PEM and a solid is such that the two are not in full (elastic) contact but are still close to each other, i.e. they may be thought of as separated by a thin airgap. This is a case which either may be modelled as described in Sect. 8.5.1, in case the airgap must be meshed as a separate domain, or in cases where this could be complicated (due to e.g. geometry) it may be modelled through an approximate boundary condition as presented below (Fig. 8.2). We use the superscript o to distinguish between the acoustic air domain previously discussed, Sect. 8.5.1, and the present domain which will only be used in an intermediate step.

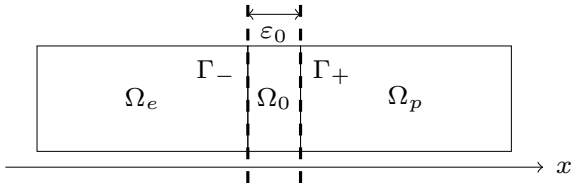

Fig. 8.2 Zoom on the region with a thin airgap separating the PEM domain from the elastic domain

At the boundary where the PEM and the airgap domain meet, here identified as Γ^-, the total stress in the PEM must equal the acoustic pressure in the airgap because of a zero *in-vacuo* stress,

$$\sigma_{ij}^{tot} n_j^p = -p^o; \quad x_i \in \Gamma^-, \tag{8.56}$$

and the pressure and the displacements have to be continuous,

$$p = p^o; \quad x_i \in \Gamma^-, \tag{8.57}$$

$$u_i^o n_i^o = (1-\phi)\, u_i^s n_i^p + \phi u_i^f n_i^p; \quad x_i \in \Gamma^-. \tag{8.58}$$

At the opposite side of the airgap domain, Γ^+, the elastic solid displacements has be equal to the acoustic displacements,

$$u_i^e n_i^e = u_i^o n_i^e; \quad x_i \in \Gamma^+, \tag{8.59}$$

and the solid stress has to be equal to the acoustic pressure in the airgap,

$$\sigma_{ij}^e n_j^e = -p^o; \quad x_i \in \Gamma^+. \tag{8.60}$$

If we now assume that the width ε_o of the airgap is very small, we can also assume that the fluid in the airgap is incompressible and the pressure thus constant in the direction normal to the boundary, $p^o = p$. Noting that $n_j^p = -n_j^o$ and assuming that ε_o goes to zero, the surface integrals pertaining to the PEM2 formulation that naturally couples to a solid, together results in,

$$\int_{\Gamma_+} \left(p n_i^p v_i^s + u_i^s n_i^p q \right) d\Gamma - \int_{\Gamma_-} \left(p n_i^p v_i^e + u_i^e n_i^p q \right) d\Gamma. \tag{8.61}$$

The boundary integrals appearing in (8.61), are also in this case standard fluid-structure interaction area integrals, here denoted by Γ_{fs}, and the assembled equation system may be written as,

$$\begin{bmatrix} [\mathbf{A}^e] & [\mathbf{0}] & -[\boldsymbol{\Gamma}_{fs}^-] \\ [\mathbf{0}] & [\mathbf{A}^{uu}] & [\mathbf{A}^{up}] + [\boldsymbol{\Gamma}_{fs}^+] \\ -[\boldsymbol{\Gamma}_{fs}^-]^T & [\mathbf{A}^{pu}] + [\boldsymbol{\Gamma}_{fs}^+]^T & [\mathbf{A}^{pp}] \end{bmatrix}, \tag{8.62}$$

where we have omitted the partitioning into interior and boundary *dof* for clarity (Fig. 8.3).

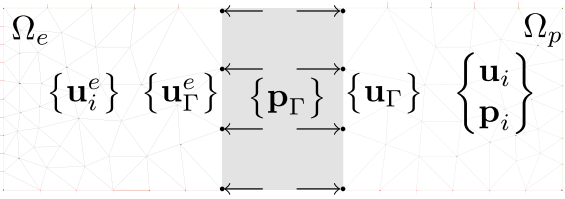

Fig. 8.3 Coupling of elastic and poroelastic FE models using an approximate representation of a thin airgap. Arrows symbolically indicate the pressure loading on the elastic solid nodes and the porous solid *dof* at the boundary

8.5.4 Coupling with Bloch Waves

We now proceed to the case where a PEM domain is coupled with a Bloch wave. Here a 2D problem is considered for a unit cell of period D and with periodic boundary conditions. In the present case, this problem is composed of two domains, an acoustic air and the second one is PEM. The PEM boundary is excited by an incident plane wave in the air domain. The components of the wave vector are $k_x = k_0 \sin(\theta)$ and $k_z = k_0 \sin(\theta)$, with k_0 the wave number in air and θ the angle of the incident wave. In the air domain, the physical fields can be represented as a superposition of the incident wave and reflected Bloch waves. The pressure p^a may then be expressed as:

$$p^a(x,z) = e^{j(k_x x + k_z z)} + \sum_{l=-\infty}^{+\infty} e^{j(k_x(l)x - k_z(l)z)} R_l, \tag{8.63}$$

where R_l are the amplitudes of the reflected Bloch waves, $k_x(l)$ and $k_z(l)$ are the x and z components, respectively in the wave vector. They are given by

$$k_z(j) = \sqrt{k_0^2 - k_x(l)^2}, \quad k_x(l) = k_x + \frac{2\pi l}{D}. \tag{8.64}$$

From Euler's equation, we can deduce the displacement of air in the z direction:

$$u_a^- = \frac{j}{\rho_a \omega^2}\left(k_z e^{j(k_x x + k_z z)} + \sum_{l=-\infty}^{+\infty} k_z(l) e^{j(k_x(l)x - k_z(l)z)} R_l\right). \tag{8.65}$$

The porous material in the FE domain is modelled by the PEM1 formulation. We recall, the boundary integral on the interface:

$$I_{FE} = \int_{\Gamma_b} v_i^s(x)\hat{\sigma}_{ij}^s(x) n_j + \frac{\phi^2}{\rho_0 \omega^2}\hat{\alpha}_{ij}\, p_{,j}(x) n_i q(x)\, \mathrm{d}\Gamma = 0. \tag{8.66}$$

In order to couple the two domains, one should consider the interface relations on Γ_b, the continuity of the pressure, of the fluid displacement and the vanishing *in-vacuo* stress:

$$p^a(x) = p(x), \quad \hat{\sigma}^s_{iz}(x) = 0, \quad u^a_z(x) = u^t_z(x) = \frac{\phi^2}{\rho_0 \omega^2} \hat{\alpha}_{zj} p_{,j}(x). \tag{8.67}$$

Using these relations, the integral I_{FE} in (8.66) may be rewritten. First, the solid term of the integral is zero due to the nullity of the *in-vacuo* stress. Concerning the pressure, it may be rewritten using the continuity of the normal displacement and the expression (8.65). We then have:

$$I_{FE} = \frac{j}{\rho_a \omega^2} \int_{\Gamma_b} \left(-k_z e^{-jk_x x} - \sum_{l=-\infty}^{+\infty} k_z(l) e^{-jk_x(l)x} R_l \right) q(x) \, \mathrm{d}\Gamma. \tag{8.68}$$

We may then deduce from this expression that the boundary term of the weak form can be expressed as a function of the amplitudes of the Bloch waves. The method then consists in considering these amplitudes as unknowns and then to add them to the degrees of freedom of the FE problem. It is first necessary to truncate the infinite sum in (8.68). The infinite sum is then approximated by considering that $l = -N_b .. + N_b$, where N_b is determined by considering classical criteria to truncate Bloch waves. The integral can be rewritten in a more condensed form:

$$I_{FE} = -\frac{jk_z}{\rho_a \omega^2} I(0) + \sum_{l=-N}^{N} \frac{jk_z(l)}{\rho_a \omega^2} I(l) R_l, \tag{8.69}$$

with

$$I(l) = \int_{\Gamma_b} e^{-jk_x(l)x} q(x) \, \mathrm{d}\Gamma, \tag{8.70}$$

and $I(l)$ is the integral of the shape function weighted by an exponential term associated with the Bloch wave. It may be discretised in a way similar to the one presented above. As it is the product of an exponential and a polynomial, its value may be computed analytically by successive integration by parts. The first term in the right hand side of (8.69) will then lead to the excitation vector. The second one will lead to a block [**B**] that will be associated to variational *dof* **q** and to the vector of unknown reflection coefficients **B**.

As $2N_b + 1$ new unknowns have been introduced, it is necessary to combine them with new constraints. This can be easily done by considering the continuity of pressure (which is the only relation in (8.66) which was not considered up to now in the derivation). First, we consider an index $m \in \mathbb{R}$, the projection of the pressure on $e^{jk_x(m)x}$ then leads to:

$$\int_{\Gamma_b} p^a(x) e^{jk_x(m)x} \, \mathrm{d}\Gamma = D\delta_{m0} + DR_m. \tag{8.71}$$

We can then discretise this relation by replacing the pressure in air by the degrees of freedom on the boundary. The discretisation of the first term in the right hand side will then lead to an excitation term and the other ones leads to a block $[\mathbf{B}']$ to be inserted in the global matrix. The final linear system is then

$$\begin{bmatrix} [\mathbf{A}^{uu}] & [\mathbf{A}^{up}] & [\mathbf{0}] \\ [\mathbf{A}^{pu}] & [\mathbf{A}^{pp}] & [\mathbf{B}] \\ [\mathbf{0}] & [\mathbf{B}'] & D[\mathbf{I}_{2N_b+1}] \end{bmatrix} \begin{Bmatrix} \mathbf{u} \\ \mathbf{p} \\ \mathbf{R} \end{Bmatrix} = \begin{Bmatrix} \mathbf{0} \\ \mathbf{F} \\ \mathbf{1}_0 \end{Bmatrix}. \tag{8.72}$$

$[\mathbf{I}_{2N_b+1}]$ is the identity matrix and $\mathbf{1}_0$ is the vector of $\mathbb{R}^{2N_b+1}$ whose first component is one and all the others are zero.

8.6 Application Examples

One of the characteristic properties of modelling of PEMs, is the intricate interactions both throughout the domain as well as at the boundary to other porous and non-porous domains. These interactions quite often tend to control the discretisation and the meshing, thus driving the size of the resulting algebraic systems to be solved. There are several reasons for this, e.g.:

- Wavelengths of the Biot waves are generally shorter than those of the acoustic or the solid waves, see [11–13]. To meet adequate mesh criteria, usually a larger mesh density or number of *dof* are required in the porous domain, as compared to the fluid or solid domains.
- The poroelastic domain is meshed by volume elements, requiring a discretisation in the 3 spatial directions (for 3D problems), unlike the elements of thin structures, such as plates or shells, which in many cases of practical interest may be meshed in 2 directions.
- The number of degrees of freedom per node of the poroelastic elements is at least 4, which together with the volume modelling required, tend to increase the model size as well as the bandwidth of the problem, [14].

From the above points we realise that the mixed-pressure formulation, having only 4 degrees of freedom per node, is interesting for many applications and we will in the following show some examples of varying complexity of its use in different modelling situations. These examples are chosen in order to illustrate the effects of boundary conditions between an PEM and a solid, as well as the effects of anisotropy, in the behaviour of different multi-layered configurations.

8.6.1 Convergence Aspects

In this section, some aspects related to the convergence of the FE model are presented. These are illustrated through a simple case, see Fig. 8.4, which consists of a 1D problem of a foam layer. The thickness of the layer is equal to 10 cm. On the left boundary, the foam is excited by plane wave of amplitude 1. On the right boundary, the porous layer is fixed and the solid displacement as well as the normal gradient of the pressure are both zero. A reflected wave with an amplitude R is then created. As R is not known, it is added to the degrees of freedom of the FE model by the way of the technique presented in Sect. 8.5.4. For this simple problem an analytical expression of the surface impedance can be derived [7, 15] from which the reflection coefficient R_t can be deduced. This analytical solution will be considered as the reference when the convergence is discussed in the following. The layer is modelled by the PEM1 formulation and the mesh consists of n element Ω_n of equal dimension. On each reference element (corresponding to $\xi \in]-1, 1[$), the solid displacement and the pressure are discretised with Lobatto shape functions. The first two orders correspond to linear shape functions:

$$\varphi_0(\xi) = \frac{1-\xi}{2}, \quad \varphi_1(\xi) = \frac{1+\xi}{2}. \tag{8.73}$$

For the higher orders $k > 1$ the shape functions are the Lobatto shape functions

$$\varphi_k(\xi) = \sqrt{k - \frac{1}{2}} \int_1^{xi} L_{k-1}(s)\, \mathrm{d}s, \quad k > 2p \tag{8.74}$$

where $L_k(\xi)$ are the Legendre polynomials and p is the order of the approximation. In each element, we then have p degrees of freedom for both the solid displacement and pressure.

We present the convergence at a single frequency, here 946 Hz, which corresponds to the resonance frequency of the solid frame. The results shown are representative also for other frequencies and the conclusions are thus frequency independent. The analysis is done by fixing the order p and refining the mesh by increasing the number

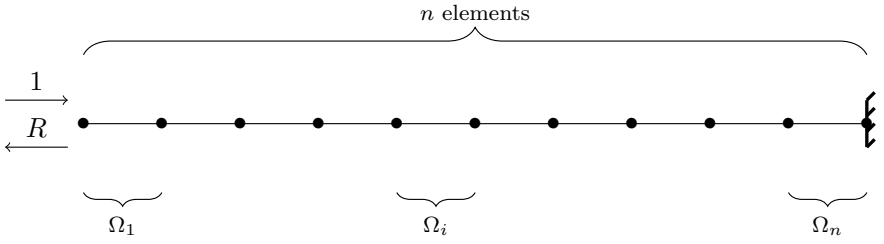

Fig. 8.4 Configuration used for the convergence analysis

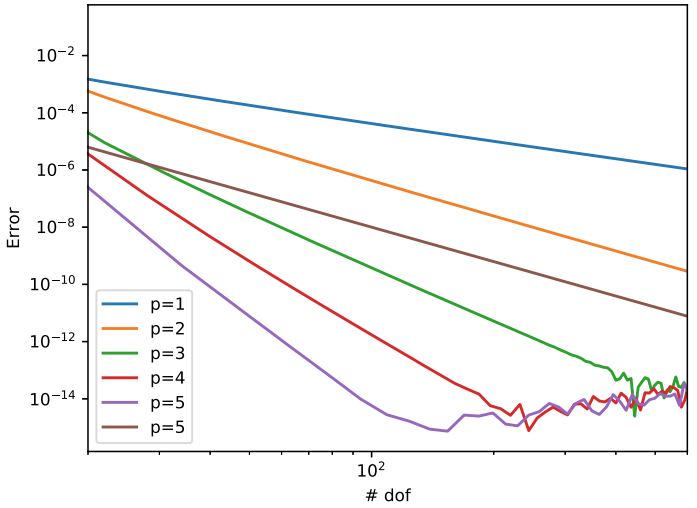

Fig. 8.5 Convergence curves for several orders

of element n of the mesh. The error ε is simply defined as the difference between the analytically and numerically computed reflection coefficients:

$$\varepsilon = |R - R_t|. \tag{8.75}$$

The result are presented in Fig. 8.5 for each order p between 1 and 5. The error is plotted as a function of the number of degrees of freedom and the results are displayed in logarithmic scale. The results obtained for a PEM follows the same trends as can be observed for other kinds of media. Starting with the case $p = 1$ i.e. linear elements, we can see that the error decreases with the number of elements but the convergence is rather slow. For $p = 2$, i.e. quadratic elements, the convergence rate is higher in the sense that the slope of the error is larger. As a more general observation, the slope is increasing with increasing order p, indicating a considerable potential for using higher order elements. However, it is not straightforward to deduce which are the optimal orders of the elements as the sparseness of the matrix system is reduced for high p. For more details, the reader can consult [8].

8.6.2 FE Cases in 1D

For the 1D example, the objectives are to illustrate and study some characteristic behaviours of the solutions to the discretised weak forms. Here we will use the PEM2 formulation to investigate the influence of contact between a PEM and an interfacing solid, which is a well-known and critical integration effect in industrial applications.

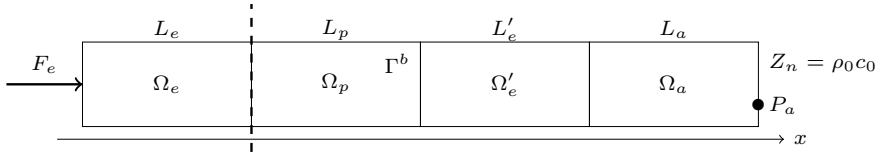

Fig. 8.6 Multilayer setup, studied as 1D example. Excitation applied to solid at the leftmost boundary and reflection free termination of acoustic domain at rightmost boundary. Along $\Gamma^{b/ub}$, either full contact or complete separation is assumed, along Γ^b full contact

The background is the difficulty in ensuring a well-defined contact between the PEM and e.g. a panel surface, as a multi-layered sound package component is manufactured. It also poses a challenging aspect in building a simulation model of such components. In addition, we emphasise that the purpose here is not to show realistic configurations and their performance, but to give the reader a deeper understanding into certain modelling aspects that should be kept in mind when building more complex and elaborate models. Thus, the physical dimensions (here thicknesses) are slightly exaggerated to allow for the visualisation to be more clear.

We take as the starting point the multilayer setup shown in Fig. 8.6, where an arrangement with two solid domains with a PEM in between, and an acoustic domain with an reflection-free termination is presented. For this example, the properties of the solid and the PEM, are given in Table 8.1. Note that we are using second order polynomials for the shape functions, see also Fig. 8.4 for a discussion of this aspect. We assume that in one case the solids are in full contact to the PEM at both boundaries, $\Gamma^{b/ub}$ and Γ^b, and in the other case that one of the solid boundaries, $\Gamma^{b/ub}$, is separated from the PEM through an airgap.
In the following we will focus on:

- The modelling as such, we will show how the airgap can be modelled either through meshing the thin acoustic domain separating the solid and the PEM, or through the approximate modelling principle taken from [16] and presented in Sect. 8.5.3.
- The effects of the airgap, illustrated through the transmission performance as well as the actual resulting fields computed at a particular frequency,

When modelling of a combination of a PEM and a solid is concerned, two extreme cases for handling of the boundary conditions may be considered. Either we choose to have full contact, or full separation with a more or less well-defined distance between the boundaries. In the case of full contact, we need to introduce the boundary conditions specified in Sect. 8.5.2. For the PEM2 formulation, this amounts to vanishing boundary integrals on both sides of the PEM, and we thus solve a problem that is equivalent in form to Sect. 8.5.2.

If we now instead assume that there is an airgap, separating the PEM from the solid, with a finite thickness, of e.g. 0.1 mm, and that we as a first choice mesh it with acoustic FE. In this case we need to introduce the conditions stated in Sect. 8.5.1 at the $\Gamma^{b/ub}$ boundary to the PEM, thus solving a problem that is equivalent in form to (8.55).

Table 8.1 Parameters of the materials used for the application examples. Note isotropic equivalent values are also given for the anisotropic properties of the foam in Sect. 8.6.4

Elastic materials				
Parameter	Units	Solid (Sect. 8.6.2)		Panel (Sect. 8.6.4) Inclusion (Sect. 8.6.3)
Density	kg.m^{-3}	2700		7800
Young's modulus	GPa	72		200
Loss factor	–	0.001		0.001
Poisson ratio	–	0.3		0.3
Isotropic foams				
Parameter	Units	Sect. 8.6.2	Sect. 8.6.3	Sect. 8.6.4 Iso equi.
Thickness	mm	100	20	42
Viscous charac. length	μm	21	214	110
Thermal charac. length	μm	50	214	740
Porosity	–	0.992	0.989	0.98
Density of frame	kg.m^{-3}	50	6.1	22.1
Loss factor	–	0.1	0.21	0.
Young's modulus	kPa	120	56.4	**100**
Poisson ratio	–	0.4	0.21	**0.4**
Flow resistivity	kPa.s.m^{-2}	26.5	8.6	**60**
Tortuosity	–	1.2	1.0	**1.3**
Anisotropic foam used in Sect. 8.6.4				
Parameter	Units	Value		
Elastic moduli, xx	kPa	40		
", yy	kPa	89 KPa		
", zz	kPa	300 KPa		
", xy	kPa	33 KPa		
", xz	kPa	37 KPa		
", yz	kPa	131 KPa		
Shear moduli, xz	kPa	26 KPa		
Shear moduli, xz	kPa	21 KPa		
Shear moduli, xz	kPa	26 KPa		
Tortuosity in x, y, z	–	1.2, 1.2, 1.5		
Flow resistivity in x, y, z	kPa.s.m^{-2}	37.5, 37.5, 67.5		

We could as well decide to use the approximate boundary condition, Sect. 8.5.3, in case we need to introduce area integral terms. These introduces the forcing of the acoustic pressure in the PEM on the solid displacements of the PEM as well as to the solid displacements of the solid. In this case we solve a problem equivalent in principle to (8.62).

8.6.2.1 Effects of Bonding 1D

It is well-known that the presence of an airgap could have a strong influence on the transmission, depending on the properties of the actual PEM. With a 0.1 mm airgap we get the results in the left part of Fig. 8.7 which are compared to the fully bonded results in the same figure. The differences between the two are clear and increases over the frequency range shown. There are several reasons for the two solutions to be different from each other, see e.g. [7, 16], one quite obvious is the change in total stiffness as the solid and the PEM are joined together. This can be observed through the slight shift of the first resonance in (8.7) (a). As the PEM is quite soft in comparison to the solid, this effect is not very large. However, for the resonance at 1850 Hz, the effect of the airgap is more significant as it tends to reduce the transmission through the panel in comparison to the bonded case. Clearly, presence of an airgap is affecting the vibroacoustic behaviour in a quite complex way which is difficult to predict a priori.

To illustrate this further, we show the effects of varying the airgap thickness in the right part of Fig. 8.7. We measure the effect in terms of the relative difference to a very thin gap of 0.01 mm thickness. Clearly, for thinner airgaps the dependence upon the airgap thickness of the transmission characteristics is reduced. For airgaps less than 1 mm, the difference in the transmitted pressure at P_a is small. For larger airgaps the transmission characteristics have a strong dependence on the actual thickness as

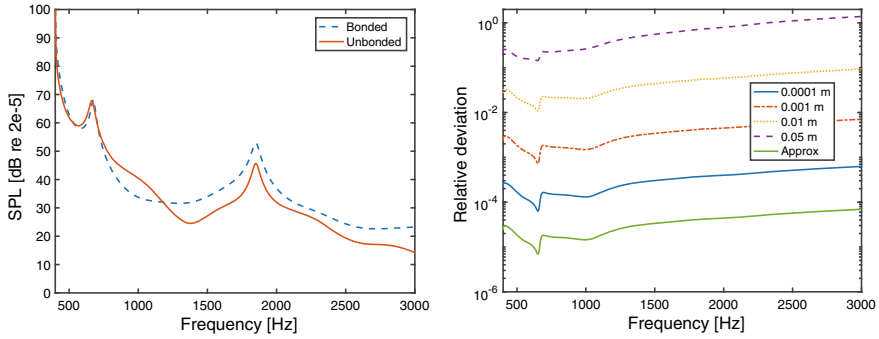

Fig. 8.7 Left: Effect of coupling conditions, bonded or unbonded, on transmitted pressure at point P_a, see Fig. 8.6, through the multilayered arrangement. Right: Relative difference in transmitted pressure at point P_a, for different airgap sizes, with 10^{-5} m used as reference gap thickness

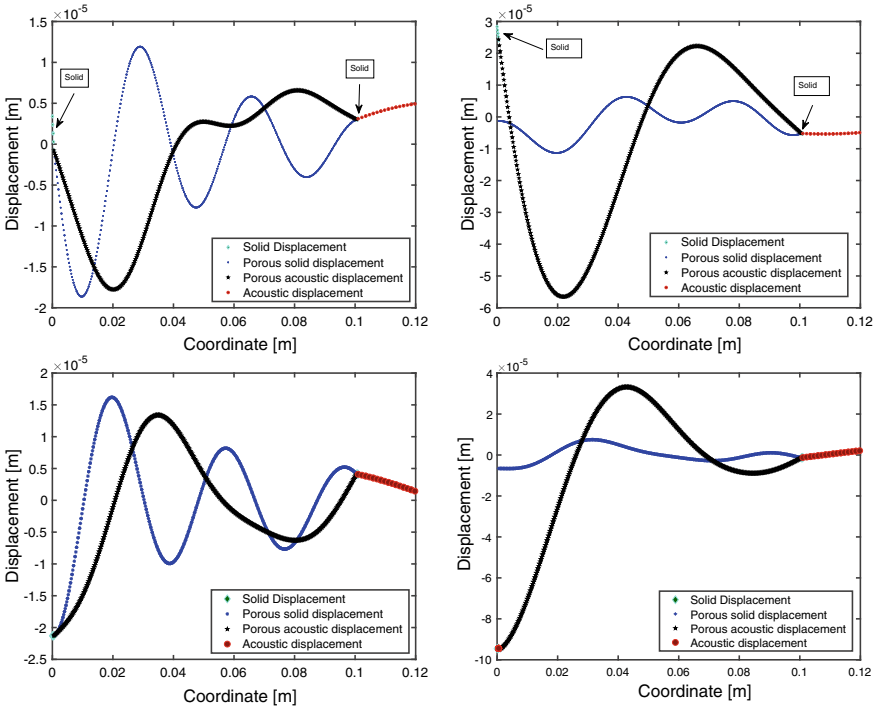

Fig. 8.8 Illustration of effects of bonding/unbonding, close-up of displacement fields inside PEM in a multilayer arrangement, real parts (top) and imaginary parts (bottom) evaluated at resonance 1850 Hz. Left: Bonded. Right: Unbonded and using approximate boundary condition

could have been expected. From Fig. 8.7, we also see that the approximate modelling represents the very thin airgap coupling well.

Let us now investigate what the effects of the airgap are in terms of the displacement fields for the solid frame and for the acoustic fluid in the PEM, see Fig. 8.8. Note that the acoustic displacements are calculated using (8.15). The different displacements are shown for the two cases considered above, i.e. bonded and unbonded. The real parts are shown in the two top sub-figures and the imaginary parts in the two bottom, with the computed displacements for the bonded to the left and unbonded to the right.

For the bonded solution, the solid frame and the acoustic fluid displacements move in phase and are identical at both boundaries, as indeed prescribed by the boundary conditions for bonding. For the unbonded solution, it is quite the opposite as the fluid displacement, at the unbonded boundary, is significantly higher than the solid frame displacement, in particular for the imaginary part. Furthermore, they are not in phase and the solid displacement is lower than the acoustic displacement at $\Gamma^{b/ub}$. Indeed, from Fig. 8.9, we see that the relative displacement $w_i = \phi(u_i^f - u_i^s)$, is higher for the unbonded case which implies a higher level of dissipation as compared to the bonded case, see (8.11)–(8.14).

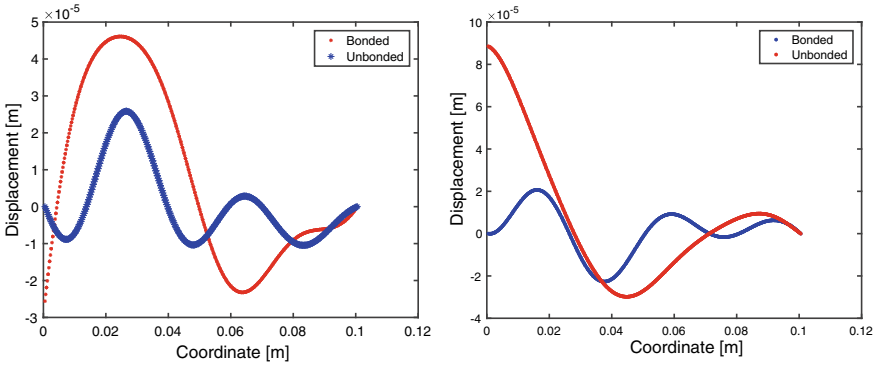

Fig. 8.9 Illustration of effects of bonding/unbonding, close-up of relative displacement fields inside PEM in a multilayer arrangement, Left: real part, right: imaginary part evaluated at resonance 1850 Hz

To conclude on this example, the approximate unbonded boundary condition represents a thin airgap well, and is an interesting alternative for complex 3D models, where the thin airgap modelling may lead to numerical problems related to elements having unacceptable aspect ratios, and where the approximation eliminates the need for meshing of the airgap through the use of boundary coupling terms instead.

8.6.3 Simulation of a Metaporous Material

A more complicated problem to solve could be a porous matrix with an inclusion. This kind of arrangement, which may involve all the different kinds of boundary conditions introduced here, is sometimes called metaporous and a 2D example is presented in Fig. 8.10. The current example is composed of a porous material Ω_p in a rectangular domain with a circular inclusion Ω_i in the center of the domain. Along Γ_t the porous medium is bonded to a rigid surface and it is excited by a plane wave on the opposite boundary, Γ_b. As this inclusion is supposed to be a part of an array of such inclusions, periodic boundary conditions are assigned along Γ_r and Γ_l boundaries, i.e. the arrangement is in fact of infinite extent in the horizontal direction. These kinds of composite structures have been the subject of extensive research in the last decade. For more details, the reader can refer to [17–22] and from these appreciate the huge variety of configurations that may be considered.

Due to the plane-wave excitation and the periodic boundary conditions, the fields in the semi-infinite lower domain are the superposition of the incident field and reflected Bloch waves. Periodic boundary conditions can be taken into account by applying the method presented in Sect. 8.6.4 and the amplitudes of the Bloch waves can be added to the FE *dof* with the method presented in Sect. 8.5.4. As the condition on Γ_t corresponds to a rigid boundary, it leads to natural boundary conditions for both PEM1 and PEM2.

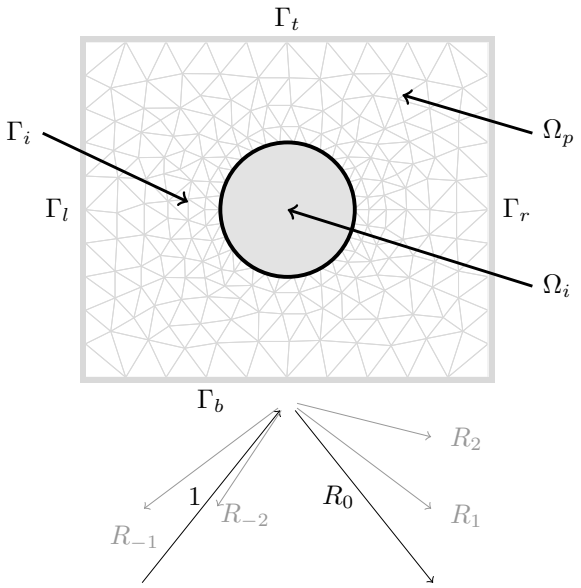

Fig. 8.10 Case of a metaporous material

Let us consider an example presented in [22]. The porous matrix is composed of foam II and has dimensions 2 cm by 2 cm. The inclusion is made of a steel material with a radius r, that will be varied in the results shown below. In this example we then have three different media: poroelastic, elastic and fluid (incident medium which is modelled by the Bloch wave superposition). Regardless of the choice of the porous formulation (PEM1 or PEM2) one of the couplings is not natural. In the results that are presented, we have chosen to use the PEM1 formulation but the results are similar for PEM2. As we have discussed previously, we then need to include a fluid-structure coupling term at the boundary Γ_i between the porous structure and the elastic inclusion. The global problem is then composed of 5×5 blocks as:

$$\begin{bmatrix} [\mathbf{A}^{ee}] & [\mathbf{A}^{e\Gamma}] & [\mathbf{A}^{eu}] & -[\boldsymbol{\Gamma}^{up}] & [\mathbf{0}] \\ [\mathbf{A}^{\Gamma e}] & [\mathbf{A}^{\Gamma\Gamma}] & [\mathbf{A}^{\Gamma u}] & [\mathbf{A}^{\Gamma p}] & [\mathbf{0}] \\ [\mathbf{A}^{ue}] & [\mathbf{A}^{u\Gamma}] & [\mathbf{A}^{uu}] & [\mathbf{A}^{up}] & [\mathbf{0}] \\ -[\boldsymbol{\Gamma}^{pu}] & [\mathbf{A}^{p\Gamma}] & [\mathbf{A}^{pu}] & [\mathbf{A}^{pp}] & [\mathbf{B}] \\ [\mathbf{0}] & [\mathbf{0}] & [\mathbf{0}] & [\mathbf{B}'] & D[\mathbf{I}_{2N_b+1}] \end{bmatrix} \begin{Bmatrix} \mathbf{u}_e \\ \mathbf{u}_\Gamma \\ \mathbf{u} \\ \mathbf{p} \\ \mathbf{R} \end{Bmatrix} = \begin{Bmatrix} \mathbf{0} \\ \mathbf{0} \\ \mathbf{0} \\ \mathbf{0} \\ \mathbf{1}_0 \end{Bmatrix}. \tag{8.76}$$

The porous matrix and the inclusion share displacement degrees of freedom $\mathbf{u}_\Gamma$ and $\mathbf{u}_e$ and $\mathbf{u}$ respectively denotes the interior degrees of freedom of the inclusion and the porous material. The upper left 3×3 corresponds to the dynamic matrix associated to the displacements. $[\mathbf{A}^{\Gamma\Gamma}]$ is assembled as the sum of a contribution from the inclusion and one of the porous material. As the PEM1 formulation does not lead to a natural coupling between fluid structure terms $[\boldsymbol{\Gamma}^{up}]$ and $[\boldsymbol{\Gamma}^{pu}]$ are introduced which are applied on the displacement of the elastic inclusion and the pressure of

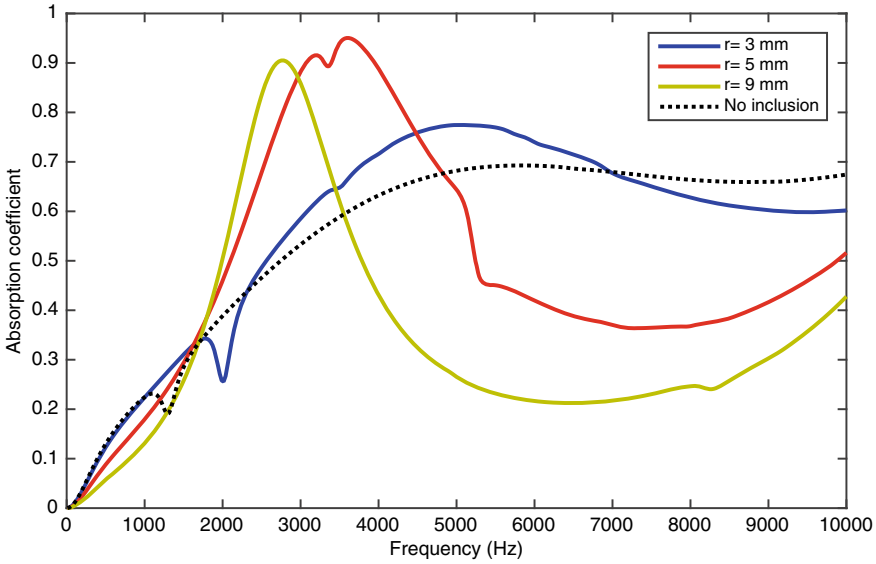

Fig. 8.11 Absorption for several different sizes of the inclusion

the porous material. Finally, the excitation introduces coupling terms [**B**] and [**B**′] between the pressure of the porous material and the reflexion coefficients. In the case of PEM1, there is no coupling term with the solid displacement.

In Fig. 8.11 the absorption coefficient for a selection of three values of the radius of the inclusion, is presented. They can be compared to the case without inclusion which is also presented. The effect of elasticity of the frame can by a localised decrease of the absorption which can be observed for example 1400 Hz in the case of an homogeneous layer 2050 Hz for $r = 3$ mm. The effect of the inclusion is to create lower frequency resonances which can increase the absorption for low frequencies. This subject is the topic of intensive researches in the last 5 years and the reader can have more details in [17, 21, 22].

The key point is that all these configurations can be modelled by the FE method. For this configuration it is also possible to derive a model based on the multiple scattering theory [22]. It is then possible to deduce an error between the two methods which is presented in Fig. 8.12. This error is mainly governed by the the mesh. In the present simulation, the mesh corresponds to 6 quadratic elements by wavelength for the shear wave. We can see that the error is mostly lower than 1%, the maximum of this error being at the resonance frequencies of the structure. The quality of the FE simulation is thus very good.

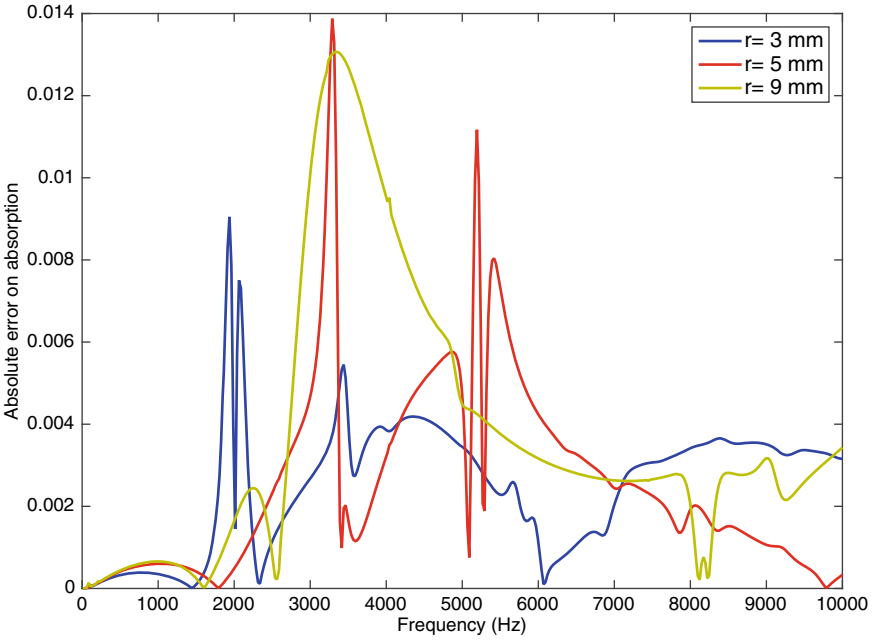

Fig. 8.12 Error between the FE method and the multiple scattering technique

8.6.4 3D Anisotropic Modelling

The effects of anisotropy of a PEM will be illustrated for a 3D example, employing the same different types of boundary conditions as discussed in the 1D case, Sect. 8.6.2. Here we use a model representing a multilayered panel, two face sheets and a PEM in between, see Fig. 8.13. Along one interface the PEM is fully bonded and along the opposite an airgap is introduced. In order to highlight the effects of anisotropy in the resulting deformations, results for an isotropic equivalent foam are also shown.

Let us first focus on the difference between the isotropic and the anisotropic PEM deformations. A significant shear deformation of the PEM is taking place in the latter, see Fig. 8.14a–b, and c–d, respectively. This is not seen in the isotropic equivalent PEM model, as there are only small Poisson's ratio effects inducing lateral deformations, and the deformation of the PEM core is almost uniaxial. This is in contrast to the anisotropic PEM model, where we see complicated shear deformations with short spatial wave lengths, in particular for the bonded case in Fig. 8.14a.

The lateral deformations are also noticeable in the presence of an airgap, see Fig. 8.14c, d. However, the difference between the isotropic and the anisotropic PEM models is slightly less. This is partially related to the release of the solid displacements at the upper panel interface, as now the coupling between the panel and the PEM

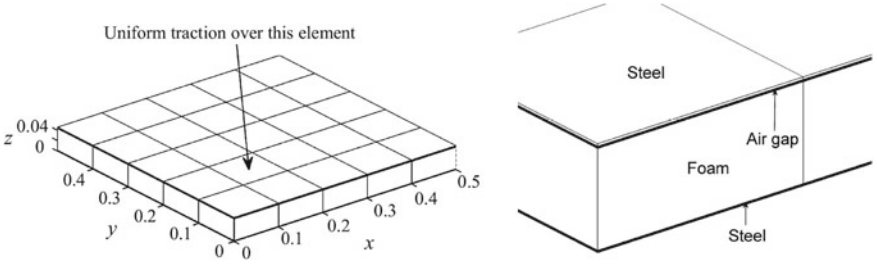

Fig. 8.13 Model problem used in 3D example of simulation of anisotropic foam formulation, parameters used in the simulations may be found in Table 8.1. For comparison, an airgap of thickness 0.001m is introduced at the upper interface between the PEM core and the face plate. Reprinted from [23] with permission

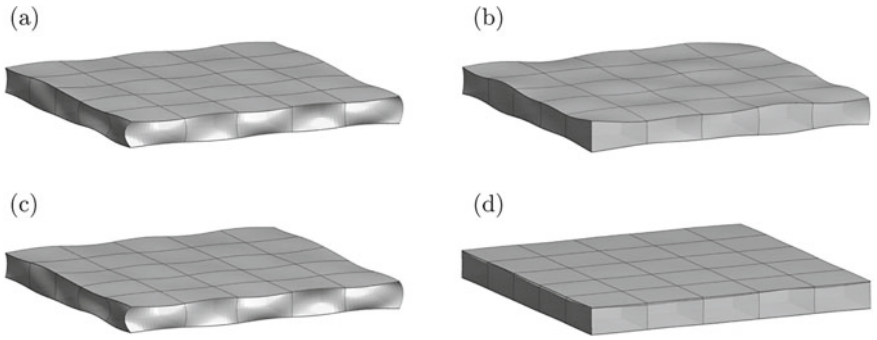

Fig. 8.14 Deformations 400 Hz. Light grey is foam core, dark is solid panel. Left: anisotropic, Right isotropic. **a** and **b** Bonded configuration, **c** and **d** Unbonded configuration. Reprinted from [23] with permission

is via the pore pressure, see Sect. 8.5.3. However, also for the airgap case, there are short wave length shear deformations in the PEM core, which are not present in the isotropic model.

We conclude from this, without giving any detailed explanations, that different waves in the anisotropic PEM are excited when the different boundary conditions are applied. This is in agreement with the simpler model studied in Sect. 8.6.2 and has been further discussed in [24] using a transfer matrix solution approach.

Acknowledgements This chapter is based upon work from COST Action DENORMS CA15125, supported by COST (European Cooperation in Science and Technology). The authors would like to acknowledge the funding and support by the following institutions: KTH Royal Institute of Technology, Centre for ECO2 Vehicle Design; University of Le Mans, Le Mans Acoustique. The authors would also like to thank Thomas Weisser for providing results relative to [22].

Appendix - Periodic Boundary Conditions

Here we review a technique for introduction of periodic boundary conditions, which is not specific to poroelasticity but included for reference as it is used in one of the examples. Note that the steps taken in this method is thus the same for the two $\{\mathbf{u}, \mathbf{p}\}$ formulations discussed here. If periodicity may be assumed, then the involved physical fields have a phase shift $\delta = e^{-jk_x L}$ between the boundaries of the unit cell, Γ_l and Γ_r. If we consider the fields of the PEM2 formulation as an illustration, we have:

$$p(\Gamma_r) = \delta p_(\Gamma_l)\, u_i(\Gamma_r) = \delta u_i(\Gamma_l)\, \hat{\sigma}^t_{ij}(\Gamma_r) = \phi \hat{\sigma}^t_{ij}(\Gamma_l)\, p_{,j}(\Gamma_r) = \delta p_{,j}(\Gamma_l). \quad (8.77)$$

We can then deduce a relation between the surface integrals on the two boundaries:

$$\int_{\Gamma_r} v^s_i \hat{\sigma}^t_{ij} n_j + \frac{\phi^2}{\rho_0 \omega^2} \hat{\alpha}_{ij}\, p_{,j} n_i q \, \mathrm{d}\Gamma = -\delta \int_{\Gamma_l} v^s_i \hat{\sigma}^t_{ij} n_j + \frac{\phi^2}{\rho_0 \omega^2} \hat{\alpha}_{ij}\, p_{,j} n_i q \, \mathrm{d}\Gamma. \quad (8.78)$$

Note that the minus sign in the right hand side is due to the outgoing normal which is opposite in Γ_l and Γ_r.

Recalling that in the general case, we need to consider the discretisation of the weak form including the volume integrals in the matrix and the integrals relative to Γ_l and Γ_r in the left hand side. Furthermore, we will distinguish between *dof* on the left and right boundaries of the unit cell as $\mathbf{X}_l$ and $\mathbf{X}_r$ and the interior degrees of freedom as $\mathbf{X}_i$. The *dof* vector, $\mathbf{X}$, will be partitioned accordingly and the discretised system may be written as:

$$\begin{bmatrix} [\mathbf{A}_{ll}] & [\mathbf{A}_{li}] & [\mathbf{A}_{lr}] \\ [\mathbf{A}_{il}] & [\mathbf{A}_{ii}] & [\mathbf{A}_{ir}] \\ [\mathbf{A}_{rl}] & [\mathbf{A}_{ri}] & [\mathbf{A}_{rr}] \end{bmatrix} \begin{bmatrix} \mathbf{X}_l \\ \mathbf{X}_i \\ \mathbf{X}_r \end{bmatrix} = \begin{bmatrix} \mathbf{F}_l \\ \mathbf{0}_i \\ \mathbf{F}_r \end{bmatrix}. \quad (8.79)$$

We now assume that the mesh interpolations on Γ_l and Γ_r are compatible, and thus the following relations hold:

$$\mathbf{X}_r = \delta \mathbf{X}_l, \quad \mathbf{F}_r = -\delta \mathbf{F}_l. \quad (8.80)$$

To proceed we need to eliminate $\mathbf{F}_l$ and this is achieved by suitable linear combinations of the parts of the matrix as follows. In the last row, we substitute tbF_r by $\delta \mathbf{F}_l$ and then multiply the whole row by δ^* (which is equal to $1/\delta$). This gives us an expression for $\mathbf{F}_l$ which may be used to rewrite the first row. The third row is replaced by the condition of periodicity on the *dof* , i.e. ($\mathbf{X}_r = \delta \mathbf{X}_l$). The system may then be reformulated as:

$$\begin{bmatrix} [\mathbf{A}_{ll}] + \delta^*[\mathbf{A}_{rl}] & [\mathbf{A}_{li}] + \delta^*[\mathbf{A}_{ri}] & [\mathbf{A}_{lr}] + \delta^*[\mathbf{A}_{rl}] \\ [\mathbf{A}_{il}] & [\mathbf{A}_{ii}] & [\mathbf{A}_{ir}] \\ \delta[\mathbf{I}_{rr}] & [\mathbf{0}] & -[\mathbf{I}_{rr}] \end{bmatrix} \begin{bmatrix} \mathbf{X}_l \\ \mathbf{X}_i \\ \mathbf{X}_r \end{bmatrix} = \begin{bmatrix} \mathbf{0}_l \\ \mathbf{0}_i \\ \mathbf{0}_r \end{bmatrix}, \quad (8.81)$$

which only has known quantities and furthermore the set of degrees of freedom is the same before and after the imposition of the periodicity. The latter is a key advantage with the above approach.

References

1. E. Deckers, S. Jonckheere, D. Vandepitte, W. Desmet, Modelling techniques for vibro-acoustic dynamics of poroelastic materials. Arch Comput Methods Eng **22**, 183–236 (2015)
2. M.A. Biot, Theory of elasticity and consolidation for a porous anisotropic solid. J Appl Phys **26**(2), 182–185 (1955)
3. M.A. Biot, Theory of propagation of elastic waves in a fluid-saturated porous solid. i. low-frequency range. J Acoust Soc Am **28**(2), 168–178 (1956)
4. M.A. Biot, Theory of stress-strain relations in anisotropic viscoelasticity and relaxation phenomena. J Appl Phys **25**(11), 1385–1391 (1954)
5. M.A. Biot, Theory of deformation of a porous viscoelastic anisotropic solid. J Appl Phys **27**(5), 459–467 (1956)
6. M.A. Biot, Mechanics of deformation and acoustic propagation in porous media. J Appl Phys **33**(4), 1482–1498 (1962)
7. J.F. Allard, N. Atalla, *Propagation of Sound in Porous Media. Modelling Sound Absorbing Materials*, 2nd edn. (Wiley, 2009)
8. N.-E. Hörlin, P. Göransson, Weak, anisotropic symmetric formulations of biot's equations for vibro-acoustic modelling of porous elastic materials. Int J Numer Methods Eng **84**(12), 1519–1540 (2010)
9. N. Atalla, R. Panneton, P. Debergue, A mixed displacement-pressure formulation for poroelastic materials. J Acoust Soc Am **104**, 1444–1452 (1998)
10. N. Atalla, M. Hamdi, R. Panneton, Enhanced weak integral formulation for the mixed (u, p) poroelastic equations. J Acoust Soc Am **109**, 3065–3068 (2001)
11. J.F. Allard, O. Dazel, J. Descheemaeker, N. Geebelen, L. Boeckx, W. Lauriks, Rayleigh waves in air saturated axisymmetrical soft porous media. J Appl Phys **106**(1) (2009)
12. P. Göransson, Tailored acoustic and vibrational damping in porous solids - engineering performance in aerospace applications. Aerosp Sci Technol **12**, 26–41 (2008)
13. P. Goransson, Acoustic and vibrational damping in porous solids. Philos Trans R Soc A - Math Phys Eng Sci **364**, 89–108 (2006)
14. O.C. Zienkiewicz, R.L. Taylor, O.C. Zienkiewicz, R.L. Taylor, *The Finite Element Method*, vol. 3 (McGraw-hill London, 1977)
15. O. Dazel, B. Brouard, C. Depollier, S. Griffiths, An alternative Biot's displacement formulation for porous materials. J Acoust Soc Am **121**(6), 3509–16 (2007)
16. P. Goransson, A 3-D, symmetric, finite element formulation of the Biot equations with application to acoustic wave propagation through an elastic porous medium. Int J Numer Methods Eng **41**(1), 167–192 (1998)
17. J.-P. Groby, B. Brouard, O. Dazel, B. Nennig, L. Kelders, Enhancing rigid frame porous layer absorption with three-dimensional periodic irregularities. J Acoust Soc Am **133**(2), 821–831 (2013)
18. C. Lagarrigue, J.P. Groby, V. Tournat, O. Dazel, O. Umnova, Absorption of sound by porous layers with embedded periodic arrays of resonant inclusions. J Acoust Soc Am **134**(6), 4670–4680 (2013)
19. J.-P. Groby, C. Lagarrigue, B. Brouard, O. Dazel, V. Tournat, B. Nennig, Using simple shape three-dimensional rigid inclusions to enhance porous layer absorption. J Acoust Soc Am **136**(3), 1139–1148 (2014)

20. J.-P. Groby, C. Lagarrigue, B. Brouard, O. Dazel, V. Tournat, B. Nennig, Enhancing the absorption properties of acoustic porous plates by periodically embedding Helmholtz resonators. J Acoust Soc Am **137**(1), 273–280 (2015)
21. C. Lagarrigue, J.-P. Groby, O. Dazel, V. Tournat, Design of metaporous supercells by genetic algorithm for absorption optimization on a wide frequency band. Appl Acoust **102**, 49–54 (2016)
22. T. Weisser, J.-P. Groby, O. Dazel, F. Gaultier, E. Deckers, S. Futatsugi, L. Monteiro, Acoustic behavior of a rigidly backed poroelastic layer with periodic resonant inclusions by a multiple scattering approach. J Acoust Soc Am **139**(2), 617–629 (2016)
23. P. Göransson, N.-E. Hörlin, Vibro-acoustic modelling of anisotropic porous elastic materials: a preliminary study of the influence of anisotropy on the predicted performance in a multi-layer arrangement. Acta Acustica united with Acustica **96**(2), 258–265 (2010)
24. J.P. Parra Martinez, O. Dazel, P. Göransson, J. Cuenca, Acoustic analysis of anisotropic poroelastic multilayered systems. J Appl Phys **119**(8), 084907 (2016)